This is a peer-reviewed, author's accepted manuscript of the following research article:
Radecka, A., Coakley, J., Vorontsov, V. A., Martin, T. L., Bagot, P. A. J., Moody, M. P., Rugg, D., & Dye, D. (2016).
Precipitation of the ordered α2 phase in a near-α titanium alloy. Scripta Materialia, 117, 81-85.
https://doi.org/10.1016/j.scriptamat.2016.02.015

Precipitation of the ordered α_2 phase in a near-α titanium alloy

A. Radecka[a], J. Coakley[b,c], V.A. Vorontsov[a], T.L. Martin[d], P.A.J. Bagot[d], M.P. Moody[d], D. Rugg[e], D. Dye[a]

[a] *Department of Materials, Royal School of Mines, Imperial College London, Prince Consort Road, London, SW7 2BP, UK*
[b] *Department of Materials Science and Metallurgy, University of Cambridge, Cambridge CB3 OF3, UK*
[c] *Department of Materials Science and Engineering, Northwestern University, 2220 Campus Drive, Evanston, IL 60208-3108, USA*
[d] *Department of Materials, University of Oxford, Oxford OX1 3PH, UK*
[e] *Rolls Royce, Elton Road, Derby, DE24 8BJ, UK*

Abstract

Precipitate evolution in a near-α alloy was studied using transmission electron microscopy (TEM) and correlative atom probe tomography (APT) after ageing at 550–700 °C for times up to 28 days. It is found that precipitation occurs much faster and is more prolific in samples heat treated at higher temperatures. Particles were spherical after ageing at 550 °C, while after ageing at 700 °C they become ellipsoids with the major axis lying close to the [0001] direction. At longer ageing times, the α_2 precipitates were found to contain greater amounts of Sn+Si, indicating that Sn and Si are stronger Ti_3(Al,Sn,Si) formers than Al.

Keywords: titanium alloys, precipitation, atom probe tomography, transmission electron microscopy (TEM)

Recent years have seen dramatic increases in the demand for commercial air travel and the cost of fuel, along with reductions in the cost of capital and the social acceptability of emissions. Strong competition has therefore driven efforts to improve the efficiency of aircraft engines [1] by running them at higher temperatures [2]. As a consequence, the materials used have to be resistant to increasingly extreme conditions. Creep resistant α Ti alloys have a high specific strength, making them ideal for high temperature compressor applications [3].

Many studies have been carried out to develop near-α Ti-Al alloys containing additions of zirconium (Zr), tin (Sn), molybdenum (Mo), niobium (Nb) and silicon (Si) [4–8]. Near-α Ti alloys are utilised for compressor discs and blades [9, 10] with improved tensile strength, fatigue resistance and creep performance at temperatures up to 660 °C [11–13]. However, as a result of solute partitioning in primary α grains, formation of the α_2 (Ti_3Al) phase has been reported [14, 15]. A detrimental effect of Ti_3Al precipitates on fracture toughness and low cycle fatigue properties is well documented [16]. Moreover, it is known that the low cycle fatigue resistance is reduced due to promotion of strain localisation as a result of the presence of α_2 [17]. It was previously reported that when slip occurs in a material containing Ti_3Al precipitates dislocations travel in pairs [18]. Cross slip is restricted and therefore deformation tends to occur by non-homogeneous planar slip [17, 18]. This is a significant problem since the resulting lowered fatigue resistance can reduce the lifetime of compressor discs [19].

IMI 834 is a near-α alloy currently deployed in high temperature compressor disc applications with a β transus temperature of 1060 °C [20]. This alloy has a reduced volume fraction of β phase with ∼15 vol.% of the fine primary α phase. This is achieved by reducing the proportion of β stabilisers, such as Mo. Sn and Zr are added as α stabilisers [21] in quantities up to 6 wt.%. Above this, embrittlement occurs due to the formation of Ti_3Al [7]. Small amounts of Si are added to increase the high-temperature strength by the formation of fine ordered precipitates on the lamella boundaries, having a stoichiometry of $(Ti,Zr)_6Si_3$ [14, 22].

IMI 834 has a good combination of creep, low cycle fatigue (LCF) and crack propagation properties, but a potential problem with this alloy is the precipitation of the α_2 phase when the solubility limit of Al is exceeded. In service, near-α Ti alloys are used for many thousands of hours at temperatures above 500 °C and it is possible that they are subjected to an uncontrolled decomposition transformation. It is worth noting that, although limited formation of the α_2 phase is sometime used in commercial Ti alloys to improve strength, the precipitation process is still not well understood. Hence, a detailed investigation of the kinetics of the formation and nucleation of α_2 precipitates in the α phase is essential for predicting the behaviour of materials at elevated temperatures.

Previous atom probe tomography (APT) and transmission electron microscopy (TEM) work on decomposition transformation in the α phase of IMI 834 has been minimal and the information on the kinetics of the transformation is still unclear. Lenssen [6] noticed the precipitation of the ordered particles in the α grains after 4 and 100 hours of ageing at 700 °C and linked this with a slight reduction in mechanical performance. After ageing for 500 hours at 700 °C much larger precipitates were observed. Although ordered regions approximately 2.5 nm in diameter and 10 nm apart were seen in the α phase after 4 hours at 700 °C, no accurate information about the chemical composition was given. Zhang et al. [23] investigated the influence of ageing time and temperature on the precipitation and growth of α_2 ordered domains in a series of alloys with compositions similar to IMI 834. It was reported that Al content and ageing temperature influenced the distribution and growth rate of the α_2 phase. The higher the Al content and ageing temperature, the quicker the observed growth of the α_2 phase.

The new generation of APT instruments, with higher detector efficiencies and wide fields of view enable this system to

*Corresponding Author. Email david.dye@imperial.ac.uk, Tel: +44 797 707 6141 (no fax).

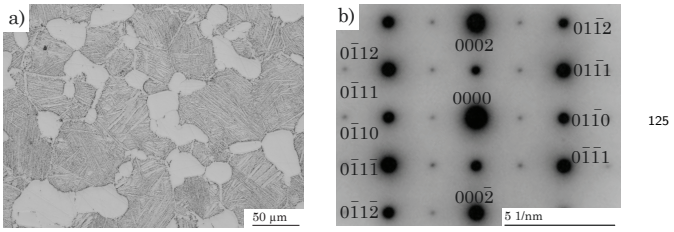

Figure 1: a) As-received bimodal microstructure and (b) Selected area [2$\bar{1}\bar{1}$0] diffraction pattern in the 625/14d sample. The intensity scale has been inverted to highlight the superlattice reflections.

be revisited, which is the focus of the current work. If large particles, like those observed by Lenssen [6], form during service, the consequences could be serious. Therefore, we examined features observed in the samples of aged IMI 834 to find out the composition of phases and the effect of ageing parameters on their nucleation and growth.

The IMI 834 material used was received from Rolls-Royce plc, of composition (measured by ICP-OES) Ti-5.8Al-4.0Sn-3.5Zr-0.7Nb-0.5Mo-0.3Si-0.10O, in wt.% (10.3Al-1.6Sn-1.8Zr-0.4Nb-0.2Mo-0.0.6Si-0.3O at.%). The alloy was forged, heat treated in the $\alpha + \beta$ phase region to give 10-15% primary α and then aged for 2h at 625 °C. The microstructure is shown in Figure 1. Small samples were then encapsulated in quartz with an Ar atmosphere and heat treated, following Lenssen [6], for 14 days at 625 °C (625/14d), 28 days at 550 °C (550/28d), 100 hours at 700 °C (700/100h) and for 16 days at 700 °C (700/16d). A larger experimental matrix was initially examined; the conditions reported here correspond to the earliest times at which some precipitation could be observed.

TEM experiments were performed using a JEOL 2000FX 200kV TEM. Samples were prepared by two methods: (i) in-situ lift out [24] and (ii) electrolytic thinning [25]. To produce specimens by the first method (i) a focussed ion beam/scanning electron microscope (FIB/SEM) Helios NanoLab 600 equipped with an Omniprobe™ was used. To prepare specimens by the second method (ii) thin slices were sectioned from the alloy, mechanically thinned down to 100 µm and discs of 3 mm diameter were cut by spark eroding. The discs were electrolytically thinned in 3% perchloric acid, 40% butan-1-ol and 57% methanol using a Tenupol-5 twin-jet electropolisher at -40 °C and a voltage between 20 and 25 V.

Atom probe samples were prepared by the FIB lift-out method. A description of the lift-out and sharpening of needle-shaped tips can be found in reference [26]. APT experiments were carried out using both a 4000X Si and 3000X HR local electrode atom probe (LEAP). The 4000X Si offers higher detection efficiencies $\sim$ 57% at the expense of mass resolution, while the 3000X HR is less efficient $\sim$ 37%, but has improved mass resolution. Each set of needles was analysed using laser and voltage-pulsing modes, in order to ensure that the observed segregation behaviour was not an artefact induced by (thermal) laser effects. The results were independent of the instrument and operating mode, but laser mode gave higher yields. A laser pulse energy of 0.1 nJ and frequency of 200 kHz were used. In voltage-pulsing mode on the LEAP 4000X Si, the voltage pulse fraction was 15%. For both modes the sample stage temperature was held at 55 K. IVAS™ data analysis software (Cameca) based on the standard algorithm [27] was used for reconstruction of the collected data [28, 29]. The iso-surface concentrations were selected to highlight the α_2 phase.

A new phase may either (i) form as a consequence of spinodal decomposition or (ii) it may form by nucleation with a long incubation time [6, 30, 31]. In the case of spinodal decomposition a compositional wave forms, which grows until a new phase is formed. In case (ii) a long incubation time can be explained by slow nucleation. To investigate the mechanism by which the new phase is formed TEM was carried out. α_2 precipitates can be identified using TEM, as they produce superlattice reflections in selected area diffraction patterns (SADP) [8]. However, it is often not possible to image precipitates using these reflections at the earliest ageing times [6, 18, 31].

Figure 1(b) shows the SADP of the 625/14d sample. The extra diffraction spots can be clearly seen, but it was not possible to image precipitates of the ordered phase in dark field (DF) mode, even with prolonged exposure times. Fundamental reflections from the matrix along with superlattice reflections were also evident in the 550/28d sample. The SADP pattern is shown in Figure 2(a). Although additional spots were clearly visible, the DF TEM images obtained using $[0\bar{1}11]_{\alpha_2}$ showed no well defined particles, but instead regions with a diffuse morphology. Therefore, the contrast seen in Figure 2(d) may be due to either regions of local order or agglomeration of small precipitates. According to Lenssen [6], superlattice diffraction spots were evident in the electron diffraction patters before compositional variation could be detected by APT. After ageing at 700 °C for several hundred hours, particles were large enough to be observed using TEM. Lenssen [6] suggested that either small ordered regions grow and become visible, or a new phase nucleated after prolonged heat treatment, possibly as the result of a compositional wave / pseudo-spinodal mechanism.

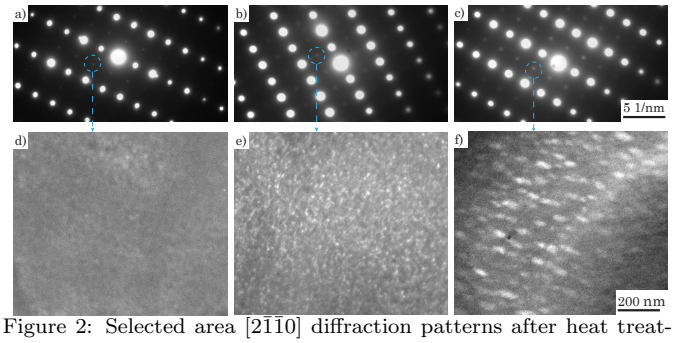

Figure 2: Selected area [2$\bar{1}\bar{1}$0] diffraction patterns after heat treatment at a) 550/28d b) 700/100h c) 700/16d. Corresponding dark-field images of the ordered regions taken from the marked superlattice spot, d), e) and f) respectively.

Table 1: APT derived phase compositions.

	Alloy		Ti	Al	Sn	Zr	Si	Nb	Mo
Matrix	550/28d	wt.%	84.9	5.8	4.4	3.2	0.2	0.6	0.8
		at.%	84.9	10.3	1.8	1.7	0.3	0.3	0.4
	700/100h	wt.%	84.2	6.9	4.2	2.7	0.4	0.7	0.7
		at.%	82.9	12.1	1.7	1.4	0.7	0.4	0.1
	700/16d	wt.%	82.4	7.1	4.7	3.4	0.6	0.9	0.7
		at.%	81.8	12.2	1.8	1.7	1.0	0.4	0.3
Particle	550/28d	wt.%	78.9	11.9	4.2	3.1	0.2	0.7	0.8
		at.%	75.3	20.2	1.6	1.6	0.3	0.3	0.4
	700/100h	wt.%	76.7	11.0	7.1	3.2	0.6	0.7	0.3
		at.%	76.8	19.0	2.8	1.6	1.0	0.4	0.1
	700/16d	wt.%	76.2	10.8	8.2	3.0	0.8	1.0	0.5
		at.%	74.2	18.7	3.2	1.5	1.3	0.5	0.2

DF TEM of the sample heat treated for 100 hours and 16 days at 700 °C clearly showed precipitates in the α phase, Figure 2(e). The microstructure of the 700/100h sample contained particles with a size of approximately 9 nm. Corresponding SADP clearly exhibit evidence of diffraction spots from the ordered phase. Similarly, in the microstructure of the sample aged for 16 days at 700 °C, particles 10×40 nm were detected. The corresponding SADP in Figure 2(f) also contained clear superlattice spots.

According to Blackburn [32], low temperature ageing of Ti-8Al wt.% (13Al at.%) produced a dispersion of the α_2 phase in the α matrix. Particles were spherical in shape up to around 50 nm and beyond this dimension they form ellipsoids with the major axis lying along the [0001] direction. A similar observation was made by Namboodhiri et al. [33] in alloys containing 8.5 and 16.5 wt.% Al (14 and 26 at.%). The authors noticed a change in morphology to an irregular shape prior to an eventual ellipsoidal geometry approximately 10 nm long. Our TEM observations are consistent with these results. In the sample that was aged for 100 hours at 700 °C particles appeared spherical, whereas after 16 days at 700 °C they possessed an elongated shape with the major axis lying along the [0001] direction. These can be clearly seen in Figure 2(e, f).

Although diffuse superlattice reflections in the SADP were observed in the sample which had been annealed for 14 days at 625 °C, APT showed only statistical fluctuations in Al concentration. The measurements were reproducible and none of the reconstructions demonstrated formation of Al-enriched regions in that sample. Additionally, no clear evidence for precipitate formation from DF TEM imaging using the superlattice spots was observed. This suggests that either the precipitates were too small to be imaged as they are outside the resolving capability of the instruments, or additional SADP spots correspond to Al rich regions formed by spinodal decomposition.

An atom map from the 550/28d APT sample is shown in Figure 3(a). This three dimensional map has a 30×120 nm cross-section. In the microstructure a high number density of small (~ 5 nm) precipitates throughout the sample is revealed. The concentration of elements was measured across interfaces, averaged over twenty similar features identified by a 14 at.% Al isosurface. The measurements were performed from the middle of the particles, in order to ensure that the value extracted from the middle corresponded only the precipitate and not to the matrix. In a classic nucleation and growth precipitation mechanism, the new phase with a sufficiently different composition would be expected to become detectable at an early stage. The fact that compositional variations are seen in APT reconstructions suggests that the contrast in TEM images is due to small particles of composition given in Table 1. It can be seen that the Al content in precipitates is greater than in the matrix by around 6 wt.%.

In Figure 3(b) atom maps from the 700/100h sample are presented. The left atom map in Figure 3(b) shows the distribution of Al atoms along with 16 at.% Al iso-concentration surfaces. At the right of Figure 3(b) a 2 nm thick slice through the data set shows the distribution of Al, Sn and Si. Sn and Si enrichment is seen in the Al-rich regions. The amount of each element was obtained from the composition profile. Figure 3(c) shows proxigrams across the boundaries of several α_2-phase precipitates. A manually selected subset was used for the composition of the matrix. Results for both the matrix and the precipitates are presented in Table 1. It can also be

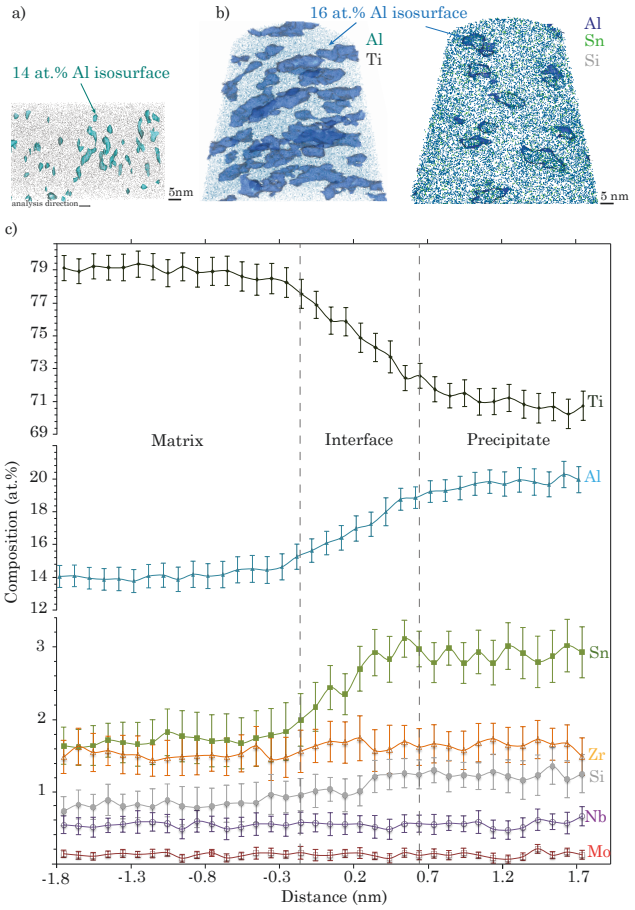

Figure 3: 3D reconstruction of the a) 550/28d on the LEAP 3000X HR and b) 700/100h sample on the LEAP 4000X Si. At right, 2 nm thick slice through the 3D reconstruction showing Al, Sn, and Si. c) Proxigram across the boundary between the aged matrix and several α_2 precipitates in the 700/100h sample.

seen clearly in the atom maps of Figure 3 that the particles have an elongated shape with the long axis between 5 and 10 nm in length.

Atom maps of the 700/16d sample are presented in Figure 4(a). After the longer ageing time at 700 °C, much bigger precipitates were observed. The particle long axis was found to be > 18 nm in length, with a short axis of ~ 7 nm. The long axis could not be measured, as the precipitates were larger than the APT sample volume. Figure 4(c) shows the integrated profile for the analysis cylinder displayed in Figure 4(b).

It can be clearly seen that Al, Sn and Si partition to the α_2 phase. The interface width is comparable with the 550/28d and 700/100h samples, around 0.8 nm. Moreover, based on the composition measurements from Table 1 it is apparent that as the extent of α_2 precipitation increases between the three samples (in the order 550/28d→700/100h→700/16d), then the Sn and Si contents increase, as does the overall Al+Sn+Si content (from 22.1 to 23.3 at.%).

Therefore, given a longer time to come to equilibrium, the Si and Sn contents increase, indicating that these are stronger α_2-formers than Al. The observation of mottled contrast at the earliest ageing times (550/28d), in the presence of strong ordering peaks in the TEM electron diffraction patterns, suggests that a distinct phase does form even before being observable by atom probe tomography. This, together with the gradual in-

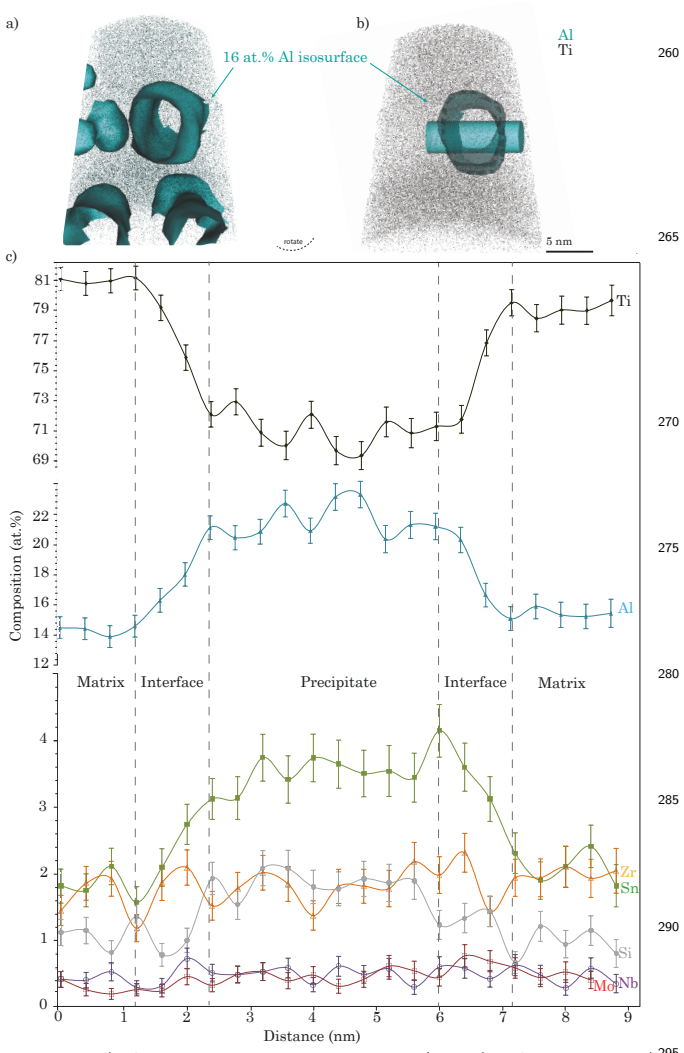

Figure 4: a) Atom probe map of the 700/16d (LEAP 4000X Si) sample showing the distribution of Ti. 4.% of detected Ti atoms are presented, with the other atoms omitted for clarity. b) Rotated view to highlight an individual precipitate - the analysis cylinder was 3 nm in diameter. (c) Composition profile along the length of the analysis cylinder in (b).

crease in the Al-site concentration (Al+Sn+Si) suggests that a spinodal-type compositional wave is associated with the transformation, as speculated by Wood et al. [30]. It is also consistent with earlier observations on the effect of Si on ordering by Woodfield [8]. Of course, the phase diagram is not of a classical spinodal form, but a classical nucleation and growth mechanism, with small precipitates first forming at the equilibrium concentration, is not indicated by the present data. The morphology change is presumably a consequence of surface (strain) energy minimisation due to the change in c/a ratio between the α and α_2 phases.

In this article, results of experiments carried out on a near-α Ti alloy IMI 834 are presented. Ordered precipitates were imaged by TEM using dark field mode with superlattice reflections. It is clearly shown by APT analyses that temperature and time affect precipitate size and morphology. At the lowest temperatures (550°C/28d, Figure 2a,d), only mottled contrast in TEM and electron diffraction spots were observed, but at longer ageing times / higher temperatures, distinct precipitates could be observed. As ageing increased, the Sn and Si contents increased, whilst the overall Al-site Sn+Si+Al content increased towards the stoichiometric composition of 25 at.%, suggesting that Sn and Si are stronger α_2-formers than Al.

Helpful discussions with Prof. T Lindley, Dr D. Isheim, Prof. D. Seidman and Prof. D. Dunand are gratefully acknowledged. The project was funded by a Rolls-Royce - EPSRC CASE studentship and by EPSRC grants RP/H004882/1 and EP/K034332/1. JC would like to acknowledge support from an EU FP7 Marie Curie fellowship.

[1] R. Boyer, JOM 62 (2010) 21-24.
[2] D. Eylon, S. Fujishir, P. Postans, F. H. Froes, JOM 36 (1984) 55-62.
[3] D. Banerjee, J. Williams, Acta Mater. 61 (2013) 844-879.
[4] N. Singh, Gouthama, V. Singh, Int. J. Fatigue 29 (2007) 843-851.
[5] N. Singh, Gouthama, V. Singh, Mater. Sci. and Eng. A 325 (2002) 324-332.
[6] L. Lenssen, FIM/atom probe study of titanium alloy, Master's thesis, Part II Thesis, Department of Materials, University of Oxford, 1987.
[7] F. Crossley, Trans. Metall. Soc. AIME 245 (1969) 1963-1968.
[8] A.P. Woodfield, P. J. Postans, M.H. Loretto, R. E. Smallman, Acta Metall., 36(3) (1988) 507–515.
[9] S. Nishikiori, H. Hattori, T. Noda, M. Okabe, S. Isobe, Mater. Sci. and Eng. A 213 (1996) 124-127.
[10] M. Somani, R. Sundaresan, O. Kaibyshev, A. Ermatchenko, Mater. Sci. and Eng. A 243 (1998) 134-139.
[11] S. Spence, W. Evans, N. Medwell, Int. J. Fatigue 19 (1997) 33-41.
[12] M. Bache, M. Cope, H. Davies, W. Evans, G. Harrison, Int. J. Fatigue 19 (1997) 83-88.
[13] P. Wanjara, M. Jahazi, H. Monajati, S. Yue, Mater. Sci. and Eng. A 416 (2006) 300-311.
[14] S. Hardt, H. Maier, H.-J. Christ, Int. J. Fatigue 21 (1999) 779-789.
[15] J. Kumar, S. Padma, B. Srivathsa, N. V. Rao, V. Kumar, J. Eng. Mater. - T ASME 131 (2009) 1012-1018.
[16] H. Rosenberg, in: The Science, Technology and Application of Titanium, 1970, pp. 851-859.
[17] M. Brandes, Creep, fatigue and deformation of α and α-β titanium alloys at ambient temperature, Ph.D. thesis, The Ohio State University, 2008.
[18] T. Neeraj, Low temperature creep of titanium alloys: Microstructure, deformation mechanisms and modeling, Ph.D. thesis, The Ohio State University, 2000.
[19] M. Sujata, N. Jagannathan, K. Raghavendra, C. M. Manjunatha, S. K. Bhaumik, JFAP 12 (2013) 437-444.
[20] E. Collings, Materials properties handbook: Titanium alloys, ASM International, 1994.
[21] M. Donachie, Titanium: A technical guide, 2nd edition ed., ASM International, 2000.
[22] C. Ramachandra, A. Singh, G. Sarma, Metall. Mater. Trans. A 24 (1993) 1273-1280.
[23] J. Zhang, Q. Wang, Y. Liu, L. Li, D. Li, JMST 20 (2004).
[24] J. Li, T. Malis, S. Dionne, Mater. Charact. 57 (2006) 64-70.
[25] D. Williams, C. Carter, Transmission electron microscopy, 2nd edition ed., Springer, 2009.
[26] G. Thompson, M. Miller, H. Fraser, Ultramicroscopy 100 (2004) 25-34.
[27] B. Gault, D. Haley, F. de Geuser, M. Moody, E. Marquis, D. Larson, B. Geiser, Ultramicroscopy 111 (2011) 448-457.
[28] D. Larson, T. Prosa, R. Ulfig, B. Geiser, T. Kelly, Local electrode atom probe tomography. A User's Guide, Springer, 2013.
[29] B. Gault, M. Moody, J. Cairney, S. Ringer, Atom probe microscopy, Springer, 2006.
[30] H. Wood, G. Smith, A. Cerezo, Mater. Sci. and Eng. A 250 (1998) 83-87.

[31] H. Liew, Short range order and phase separation in Ti-Al alloys, Ph.D. thesis, University of Oxford, 1999.
[32] M. Blackburn, Trans. Metall. Soc. AIME 239 (1967) 1200-1208.
[33] T. Namboodhiri, C. McMahon, H. Herman, Metall. Trans. 4 (1973) 1323-1331.